Theoretical Optical Waveguide Investigation of Self-Organized Polymer Thin Film Nanostructures with Nanoparticle Incorporation

King Hang Aaron Lau and Wolfgang Knoll

Max-Planck-Institute for Polymer Research, Ackermannweg 10, 55128 Mainz, Germany

Dong Ha Kim*

Max-Planck-Institute for Polymer Research, Ackermannweg 10, 55128 Mainz, Germany
Division of Nano Sciences & Department of Chemistry, Ewha Womans University, Seoul 120-750, Korea

Abstract: Hybrid thin film nanostructures composed of metal nanoparticles (NPs) and self-assembled polymer films with different spatial distributions of NPs were analyzed by optical waveguide spectroscopy (OWS). Specifically, the dielectric constants were calculated using effective medium theory for the incorporation of 1 vol% Au NP into the block copolymer (BCP) films having a cylindrical nanodomain morphology. Three cases were considered: uniform distribution of NPs in the film; selective distribution of NPs only in the cylindrical domains; and segregation of NPs to the center of the cylindrical domains. The optical waveguide spectra derived from the calculated dielectric constants demonstrate the feasibility of experimentally distinguishing the composite nanostructures with different inner morphologies in the hybrid metal NP-BCP nanostructures, by the measurement of the dielectric constants using OWS.

Keywords: block copolymers, nanoparticles, optical waveguide, thin films, effective medium theory.

Introduction

Among numerous bottom-up routes to nanostructured materials, block copolymer (BCP) self-assembly has attracted growing attention due to the ability to self-organize to form periodic arrays with lattice spacing in the range of 10-100 nm.[1,2] This unique class of polymers has been widely utilized in various applications including microelectronics, optics, and optoelectronics.[3-5] Although single polymers or organic-inorganic hybrid materials have been reported to act as patterned waveguides successfully, practical use of BCPs for waveguide applications is still limited.[6,7] To date, common analytical techniques like electron and scanning probe microscopies, and scattering techniques have been employed for the structural characterization of BCP morphologies.[8-10] However, conventional methodologies generally have major drawbacks in terms of tedious sample preparation, limited sensitivity, investigation limited to the sample surface, or the use of large scale facilities with synchrotron source, etc.

We recently demonstrated that BCP thin films can act as slab waveguides and that their dielectric constants and their thickness can be independently measured using optical waveguide spectroscopy (OWS).[11,12] In particular, depend-

ing on the shape and volume fraction of the constituent domains, the interaction of the incidence electric field with the nanostructure is correspondingly modified. This is manifested in the macroscopically measured dielectric constant even though no sub-wavelength features can be directly imaged. Effective medium theory (EMT) can then be used to fit the measured dielectric response with models of the film nanostructure and polymer composition.[11-14]

In this report, we examine the potential of OWS for analyzing nanostructures of BCP thin films. Specifically, using EMT, we calculate the dielectric constants of hybrid, metal nanoparticle-BCP composite thin films with cylindrical microdomain morphology, and predict the OWS waveguiding response. Nanoparticles have attracted much scientific interests due to their novel properties and applications.[15,16] The combination of BCP and nanoparticles may offer great potential in creating new materials or devices.[17,18] We consider cases where metal nanoparticles are incorporated selectively into different regions of the BCP nanostructure, for which several experimental approaches have been suggested already.[19,20] We consider small volume fractions of nanoparticle incorporation (1 vol%) such that normal BCP nanostructures can be induced from cooperative self-assembly. Furthermore, in this dilute limit, EMT predictions are less model-dependent,[14,21] leading to reliability of the predicted results.

---

*Corresponding Author. E-mail: dhkim@ewha.ac.kr
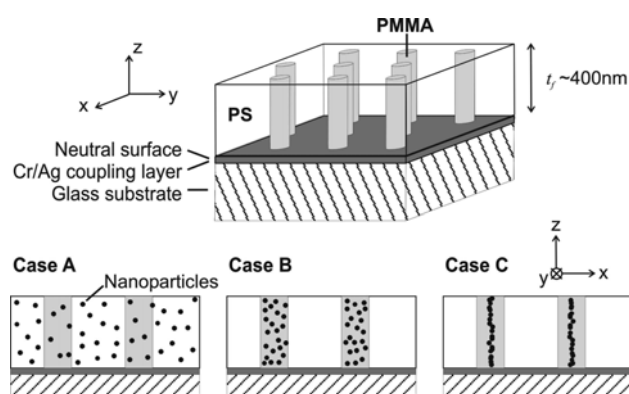
Figure 1. 3D schematic illustration of the basic PS-*b*-PMMA/hPMMA nanostructured thin film into which Au nanoparticles are incorporated. Cases A to C show the different distributions of nanoparticles considered.

BCP Model Thin Films

Figure 1 shows the basic geometry of our previously reported[11,12] BCP thin film with cylindrical morphology, along with the three hypothetical cases of nanoparticle incorporation considered in this study. The BCP system is polystyrene-*block*-poly(methyl methcrylate) (PS-*b*-PMMA) with the incorporation of poly(methyl methcrylate) homopolymer (hPMMA) in a ratio of PS : PMMA : hPMMA = 65 : 28 : 7. hPMMA self-segregates to the center of PMMA domains and fosters self-assembly of PMMA cylindrical morphology for film thickness (t_f) up to ~10 times the lattice spacing of the hexagonal cylinder array (L_o~40 nm).[22] For the hybrid nanoparticle-BCP structures considered, the amount of Au nanoparticle incorporation is fixed to 1 vol% for all cases. Case A refers to Au nanoparticles randomly distributed in the film; case B refers to Au nanoparticles selectively incorporated in PMMA cylindrical domains; and in case C, Au nanoparticles are segregated to the center of cylindrical domains to form Au nanorods. In cases B and C, the actual Au concentration within PMMA is 2.8% because Au is only incorporated in the PMMA domains. This translates to, in case B, an inter-particle separation of ~2 times the particle diameter.

In all cases the BCP film is structurally symmetric under rotation about the z-axis (considering that an actual film would consist of a number of grains with defect-free hexagonally ordered cylinders over ~1 μm^2 area oriented in different directions.). Thus the dielectric response also has the corresponding anisotropy, and we define:

$$\begin{cases} \varepsilon_x = \varepsilon_y \equiv \varepsilon^\perp \\ \varepsilon_z \equiv \varepsilon^{//} \end{cases} \quad (1)$$

Optical Waveguide Spectroscopy (OWS)

The excitation of optical waveguide modes is sensitive to
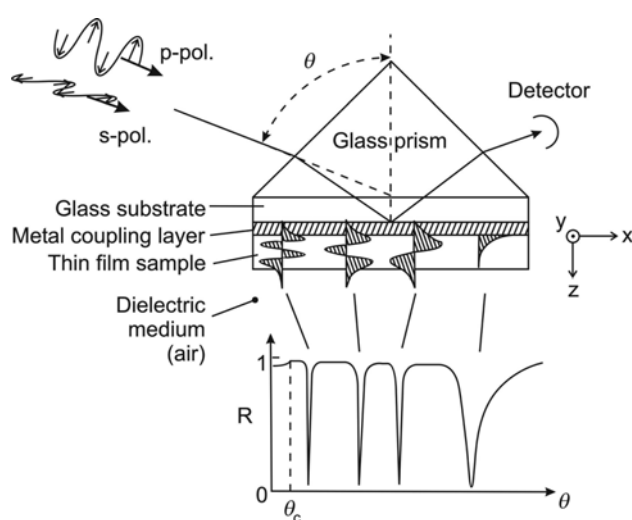
Figure 2. OWS in the Kretschmann configuration. Electric field distributions of waveguide modes, excited at different θ, are schematically shown as area curves within the sample film. The corresponding minima, as would be measured in a R vs. θ scan, are shown at the bottom. θ_c is the angle of total internal reflection for the glass-air interface.

minute changes in the dielectric constant (ε) and thickness (t_f) of the waveguiding layer. OWS operating in the Kretchmann configuration (Figure 2) is a simple set-up suited for the investigation of thin films.[23] The sample film is prepared on a glass substrate coated with a semi-transparent metal coupling layer and mounted onto a prism in a θ - 2θ angle scanning assembly. Through the back of the metal layer, light is coupled into the sample film. The sample film is an optical cavity, and if thick enough (> 200 nm for typical polymers in air), resonant waveguide modes can be excited at specific incidence angles (θ). Performing an angle scan while measuring the reflected intensity (R) reveals the resonant waveguide coupling modes as sharp intensity minima (Figure 2).

Waveguide modes can be excited with an electric field polarized either perpendicular or parallel to the film surface (p- and s-polarizations, respectively). Therefore, structural anisotropy in the film, which leads to anisotropy in the dielectric response, can be detected as differences in waveguiding behaviour under different polarizations.

In the configuration outlined, the sample is a slab waveguide in a 1D multilayer system described by $\varepsilon = \{\varepsilon_x = \varepsilon_y = \varepsilon^\perp, \varepsilon_z = \varepsilon^{//}\}$ and thickness of each layer. Maxwell's equations can be solved for the system and the reflected intensity at varying incidence angle θ is given by the Fresnel equations. Parameters for the sample layers may be obtained by fitting Fresnel's calculations to R vs. θ measurements.[23] Throughout this paper, the discussion will refer to the use of a 43 nm thick Ag film with a 3 nm Cr adhesion layer, and high index LaSFN9 glass prism with $\varepsilon = 3.406$.

Effective Medium Theory (EMT)

EMT predicts the macroscopic (effective) dielectric response (ε_{eff}) of a composite material based on the dielectric properties and morphology of the constituent phases. In general, the infinite wavelength approximation is applied, which is valid for a domain size to wavelength ratio < 1/10.[13,24] This condition is easily met for BCP structures and for nanoparticles, when probed with wavelengths in the visible or longer.

We have applied the Maxwell-Garnett approach (MG-theory)[5,26] in our analysis, which describes embedded domains (*d*) of one material completely surrounded by another matrix material (*m*):[13]

$$\varepsilon_{eff} = \varepsilon_m \frac{\varepsilon_m + (f_d + f_m q)(\varepsilon_d - \varepsilon_m)}{\varepsilon_m + f_m q(\varepsilon_d - \varepsilon_m)} \quad (2)$$

where *f* is the volume fraction, and *q* is the average screening parameter ($0 \le q \le 1$) under which any size, shape and orientation effects are subsumed.[13,14]

In the case of PS-*b*-PMMA/hPMMA films probed by p-polarization, both the cylindrical domains and the incidence electric field are aligned to the surface normal. In this case, $q \to 0$, and $\varepsilon^{\perp} = \varepsilon_{eff}(q = 0)$ is the weighted average of ε_d and ε_m. When probed with s-polarization, the incidence electric field is perpendicular to the array of cylindrical PMMA domains, in which case $q = 1/2$ and $\varepsilon^{//} = \varepsilon_{eff}(q = 1/2)$. For uniform nanoparticle incorporation in a matrix (3D isotropy), $q = 1/3$.[13,14]

In case C, the structure and dielectric response of a cylindrical domain with a string of Au particles embedded in the center are clearly anistropic. MG theory has also been extended to such geometry.[27] When probed under p-polarization, $\varepsilon^{\perp} = \varepsilon_{eff}(q = 0)$ holds as before, except that the axial component of the cylinder dielectric constant ($\varepsilon_{cyl.}^{axial}$) is used. However, when probed under s-polarization, the following relation applies:

$$\varepsilon^{//} = \varepsilon_{PS} \frac{(\varepsilon_{cyl.}^{radial} + \varepsilon_{PS}\Delta) + f_{cyl.}(\varepsilon_{cyl.}^{radial} - \varepsilon_{PS}\Delta)}{(\varepsilon_{cyl.}^{radial} + \varepsilon_{PS}\Delta) - f_{cyl.}(\varepsilon_{cyl.}^{radial} - \varepsilon_{PS}\Delta)}, \quad \Delta = \sqrt{\frac{\varepsilon_{cyl.}^{radial}}{\varepsilon_{cyl.}^{axis}}} \quad (3)$$

The basic assumptions of the MG theory are only valid for low concentrations of the inclusion phase (< 10~30%),[13,27] especially in the case of films with high dielectric contrast between the inclusions and the matrix.

In a different approach, Bruggeman[28] considered a very different, randomly intermixed microstructure for which there is no continuous matrix, and which is generally more applicable for intermediate *f*'s:[13,14]

$$0 = \frac{f_a q(\varepsilon_a - \varepsilon_{eff})}{\varepsilon_{eff} + q(\varepsilon_a - \varepsilon_{eff})} + \frac{f_b q(\varepsilon_b - \varepsilon_{eff})}{\varepsilon_{eff} + q(\varepsilon_b - \varepsilon_{eff})} \quad (4)$$

where *a* and *b* are the two materials in the composite.
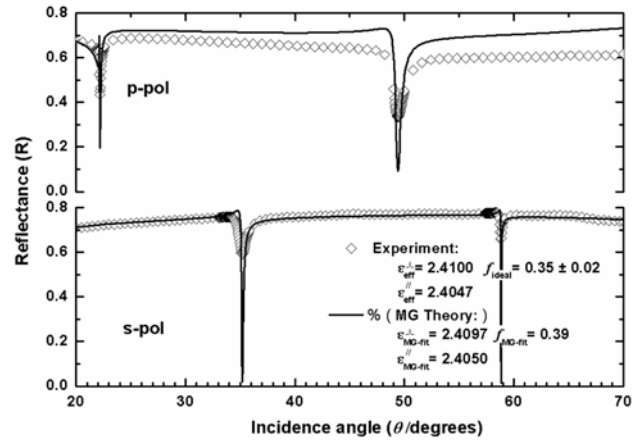
Figure 3. *R* vs. θ scan for a 464 nm thick PS-*b*-PMMA film with cylindrical PMMA domains (diamonds), fitted with MG theory calculation (line). f_{MG-fit} is varied to give values of ε_{MG-fit} that best fit ε_{eff} measured by OWS. f_{ideal} is the volume fraction of PMMA in the polymer solution used for sample preparation.

EMTs are commonly evaluated over a wide range of wavelengths. However, waveguide modes are usually excited at only one wavelength in OWS. We shall assume $\lambda = 632.8$ nm (HeNe laser) throughout this study.

To illustrate how EMT can be applied to OWS experiments, we first compare a *R* vs. θ scan for a PS-*b*-PMMA/hPMMA film ($t_f = 464$ nm)[11] with MG theory fitting as shown in Figure 3. As described above, the s-polarization plot was fitted with eq. (2) using $q = 1/2$, and the p-polarization plot was fitted using $q = 0$. The fitted ε values are inserted into Fresnel equations to generate *R* vs. θ curves. Excellent agreement is achieved in the fitting of waveguide mode coupling angles, and there is a fair agreement in the fitted volume fraction (f_{MG-fit}) compared to the ideal volume fraction (f_{ideal}) in the polymer solution used in sample preparation.

EMT and Optical Spectra Predictions

$\varepsilon^{\perp}$ and $\varepsilon^{//}$ were calculated for cases A to C by the MG approach and the results are displayed in Table I. We assume $t_f = 400$ nm. For case A, eq. (2) was first used to calculate ε_{eff} for both PS and PMMA filled with 1 vol% Au nanoparticles, by assuming $q = 1/3$. Then using PS-1%Au as the matrix and PMMA-1%Au as the cylindrical phase, eq. (2) was reapplied to calculate $\varepsilon^{\perp} = \varepsilon_{MG}(q = 0)$ and $\varepsilon^{//} = \varepsilon_{MG}(q = 1/2)$ for the cylinder array geometry. The calculation for case B is analogous to that for case A, but with PS as the matrix and PMMA-2.8%Au as the cylinder domains. For case C, the dielectric response of the PMMA-Au cylinder is anisotropic. Therefore we first calculate the dielectric constant of the cylindrical domains in the radial direction, $\varepsilon_{eff}^{radial}$, by applying eq. (2) using $q = 1/2$, ε_{PMMA} and ε_{Au}; and
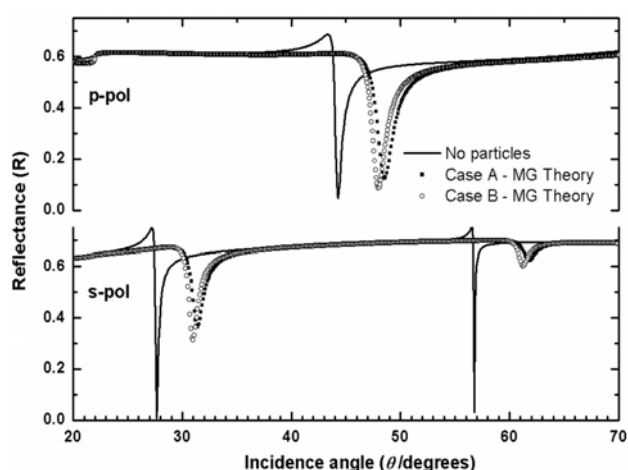
Table I. Calculated Dielectric Constants of Hybrid Au Nano-Particle/PS-*b*-PMMA Films. Dielectric Constants Used are[29,30]: $\varepsilon_{PS} = 2.53$; $\varepsilon_{PMMA} = 2.22$; $\varepsilon_{Au} = -11 + 1.33i$

Total Au vol% = 1%	$\varepsilon^{\perp}$ (normal to surface)	$\varepsilon^{//}$ (parallel to surface)
No particles	2.422	2.417
Case A (MG-theory)	$2.580 + 0.019\,i$	$2.575 + 0.019\,i$
Case B (MG-theory)	$2.559 + 0.015\,i$	$2.558 + 0.014\,i$
Case C (MG-theory)	$2.287 + 0.013\,i$	$2.373 + 0.010\,i$
Case C (Distributed)	$2.461 + 0.138\,i$	$2.473 + 0.137\,i$

Figure 5. Optical waveguide spectra calculated for case C (dashed line) compared with the same film with no particles (line). Case C-distributed (open squares) refers to incomplete Au nanoparticles segregation to the center of PMMA domains. Film thickness is 400 nm for all cases.
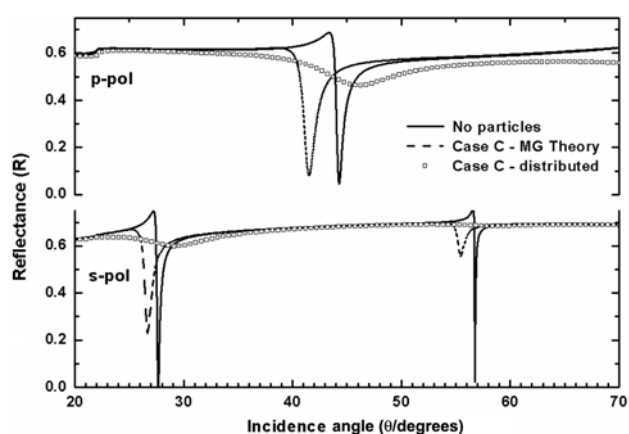
along the cylinder axis, ε_{eff}^{axis}, using $q = 0$. For the combined film, $\varepsilon^{\perp}$ was obtained from ε_{eff}^{axis}, ε_{PS}, and applying equation 2 ($q = 0$). $\varepsilon^{//}$ was obtained from eq. (3).

A compact string of Au nanoparticles might be difficult to realize experimentally. Therefore we also considered "case C-distributed" where there is a Gaussian distribution of particles centred about the axis of the cylindrical domain. We assume that half of the nanoparticles are concentrated within a central cylindrical region with a diameter 1/4 of the whole PMMA domain. We segment this distribution into 5 concentric regions each of which is decorated with uniform nanoparticle content and apply the EMT procedure to successive layers. The highest concentration of particles in the centre is 26% where MG theory is likely to break down. Thus for segments with concentrations > 10%, we used the Bruggeman approach.

Optical waveguide spectra (R vs. θ) were derived based on the values listed in Table I. Figure 4 shows the spectra for cases A and B compared with the unloaded BCP film. In both cases A and B, the dielectric constants, thus the waveguide mode coupling angles, are shifted to far higher values in-

duced by the dilute Au inclusions, reflecting the large complex dielectric constant of Au nanoparticles. Conversely, we did not observe appreciable changes from dielectric particles at this concentration (data not shown). The minima for cases A and B are also shallower than for the unloaded BCP film, indicating increased absorption due to the metallic nature of the nanoparticles. This effect is especially pronounced under s-polarization because of additional screening effects of the cylindrical morphology (EMT does not consider scattering effects.). The angular shifts are very large ($4°\sim5°$) relative to the typical angle resolution of $\sim10^{-3}$ degrees in OWS, and the spectra between the original and Au nanoparticle loaded films can be unambiguously distinguished.

Figure 5 shows the comparison between case C and the unloaded film. It is interesting to observe that waveguide coupling minima are shifted to lower angles. Since the nanoparticles are concentrated to form quasi-1D nanorods, the incidence electric field is minimally perturbed by the Au incorporation and there is a more direct averaging of the dielectric response of the polymer with the negative real part of ε_{Au}. In contrast, in cases A and B, since the Au nanoparticles are dispersed in the polymer matrix, the higher polymer-Au interfacial area and the spherical geometry contribute to higher ε_{eff} and coupling angles. This effect is most pronounced for case A, because the nanoparticles are distributed uniformly throughout the entire film. Thus the magnitudes of dielectric constants are in the following order: case A > case B > neat BCP film > case C.

Case C-distributed, also shown in Figure 5, shows what might be expected if segregation of the Au nanoparticles to the center of the PMMA domains is incomplete. As expected, the dielectric constants and waveguide coupling angles for case C-distributed are in between those of cases B and C, because as the Au nanoparticles in case C become

Figure 4. Optical waveguide spectra calculated for cases A and B (squares and open circles, respectively), compared with the same film with no particles (line), based on MG theory (Table I). Film thickness is 400 nm for all cases.

less concentrated to the center of the cylindrical domains, the structure approaches that of case B. In fact, comparison of the coupling angles of a sample with calculations based on the ideal cases of B and C could be a measure of the degree of Au nanoparticle segregation to the center of PMMA domains.

The angle minima for case C-distributed are the most broad and shallow among all structures (highest absorption). This observation results from the high effective concentration of Au at the centre of the PMMA domains (26%), but the effect could simply be due to limitations of the EMT model as one departs from the dilute limit.

Conclusions

For a set of model, PS-*b*-PMMA thin films exhibiting self-assembled cylindrical morphology with 1 vol% Au nanoparticle incorporation, dielectric constants were calculated using EMT. It was found that nanostructured films with Au particles dispersed throughout the whole film, and those with selective incorporation in the PMMA domains, display similar dielectric constants that are significantly larger than that of the neat BCP film. On the other hand, selective Au inclusion at the centre of cylindrical PMMA domains exhibits significantly smaller dielectric constants than the unloaded nanostructure.

OWS spectra derived from EMT results also illustrate this marked contrast, and demonstrate the feasibility of using OWS to predict and verify nanostructures of hybrid metal nanoparticle-BCP thin films by optical measurements of film dielectric constants, notwithstanding inaccuracies inherent in EMT modeling. More detailed and accurate optical investigations may be obtained by measurements using laser light over a range of wavelengths.[3,24] Moreover, numerical approaches to EMT,[31,32] combined with the present analytical study, may allow for more accurate predictions of the dielectric response of the model nanostructures.

Hybrid nanoparticle-polymer thin films, such as the ones analyzed in this study, may act as important components in advanced photonics and nanotechnology. Our results indicate that, through measurement of the dielectric constants, OWS can serve as a relatively simple, non-destructive optical technique to characterize the nanostructure of BCP thin films. Moreover, our calculations also demonstrate that predictions of optical properties of these nanohybrids in terms of distribution of nanoparticles is possible in advance of experimental studies, and could guide the fabrication and testing of such advanced polymer films.

References

(1) I. W. Hamley, *The physics of Block Copolymers*, Oxford University Press, New York, 1998.

(2) G. H. Fredrickson and F. S. Bates, *Annu. Rev. Mater. Sci.*, **26**, 501 (1996).

(3) M. Lazzari and M. A. López-Quintela, *Adv. Mater.*, **15**, 1583 (2003).

(4) I. W. Hamley, *Angew. Chem. Int. Ed.*, **42**, 1692 (2003).

(5) A. M. Urbas, M. Maldovan, P. DeRege, and E. L. Thomas, *Adv. Mater.*, **14**, 1850 (2002).

(6) S.-H. Nam, J.-W. Kang, and J.-J. Kim, *Macromol. Res.*, **14**, 114 (2006).

(7) K. B. Yoon, *Macromol. Res.*, **12**, 290 (2004).

(8) M. A. van Dijk and R. van den Berg, *Macromolecules*, **28**, 6773 (1995).

(9) Y. Wang, R. Song, Y. S. Li, and J. S. Shen, *Surf. Sci.*, **530**, 136 (2003).

(10) Z. Sun, D. H. Kim, M. Wolkenhauer, G.-G. Bumbu, W. Knoll, and J. S. Gutmann, *Chem. Phys. Chem.*, **7**, 370 (2006).

(11) D. H. Kim, K. H. A. Lau, W. Joo, J. Peng, U. Jeong, C. J. Hawker, J. K. Kim, T. P. Russell, and W. Knoll, *J. Phys. Chem. B*, **110**, 15381 (2006).

(12) D. H. Kim, K. H. A. Lau, J. W. F. Robertson, O.-J. Lee, U. Jeong, J. I. Lee, C. J. Hawker, T. P. Russell, J. K. Kim, and W. Knoll, *Adv. Mater.*, **17**, 2442 (2005).

(13) D. E. Aspnes, *Thin Solid Films*, **89**, 249 (1982).

(14) C. G. Granqvist and O. Hunderi, *Phys. Rev. B*, **18**, 2897 (1978).

(15) S. Eustis and M. A. El-Sayed, *Chem. Soc. Rev.*, **35**, 209 (2006).

(16) M. E. Franke, T. J. Koplin, and U. Simon, *Small*, **2**, 36 (2006).

(17) D. H. Kim, X. Jia, Z. Lin, K. Guarini, and T. P. Russell, *Adv. Mater.*, **16**, 702 (2004).

(18) J. F. Berret, N. Schonbeck, F. Gazeau, D. El Kharrat, O. Sandre, A. Vacher, and M. Airiau, *J. Am. Chem. Soc.*, **128**, 1755 (2006).

(19) X. Li, P. Göring, E. Pippel, M. Steinhart, D. H. Kim, and W. Knoll, *Macromol. Rapid Comm.*, **26**, 1173 (2005).

(20) S. Horiuchi, T. Fujita, T. Hayakawa, and Y. Nakao, *Langmuir*, **19**, 2963 (2003).

(21) C. G. Granqvist and O. Hunderi, *Phys. Rev. B*, **16**, 3513 (1977).

(22) U. Jeong, D. Y. Ryu, D. H. Kho, J. K. Kim, J. T. Goldbach, D. H. Kim, and T. P. Russell, *Adv. Mater.*, **16**, 533 (2004).

(23) W. Knoll, *Annu. Rev. Phys. Chem.*, **49**, 569 (1998).

(24) G. L. Hornyak, C. J. Patrissi, and C. R. Martin, *J. Phys. Chem. B*, **101**, 1548 (1997).

(25) J. C. Maxwell-Garnett, *Philos. Trans. R. Soc. London*, **203**, 385 (1904).

(26) J. C. Maxwell-Garnett, *Philos. Trans. R. Soc. London*, **205**, 237 (1906).

(27) F. J. García-Vidal, J. M. Pitarke, and J. B. Pendry, *Phys. Rev. Lett.*, **78**, 4289 (1997).

(28) D. A. G. Bruggeman, *Ann. Phys. (Leipzig)*, **24**, 636 (1935).

(29) L. G. Schulz, *J. Opt. Soc. Am.*, **44**, 357 (1954).

(30) L. G. Schulz and F. R. Tangherlini, *J. Opt. Soc. Am.*, **44**, 362 (1954).

(31) M. Maldovan, M. R. Bockstaller, E. L. Thomas, and W. C. Carter, *Appl. Phys. B*, **76**, 877 (2003).

(32) O. J. F. Martin and N. B. Piller, *Phys. Rev. E*, **58**, 3909 (1998).